TISSUE ENGINEERING
Volume 9, Number 3, 2003

Macroporous Biphasic Calcium Phosphate Scaffold with High Permeability/Porosity Ratio

SHIHONG LI, Ph.D.,[1] JOOST R. DE WIJN, Ph.D.,[1,2] JIAPING LI, M.Sci.,[1] PIERRE LAYROLLE, Ph.D.,[1] and KLAAS DE GROOT, Ph.D.[1,2]

ABSTRACT

Macroporous biphasic calcium phosphate (BCP) with channel-shaped pores was produced by a novel dual-phase mixing method. The processing route includes mixing water-based BCP slurry and polymethylmethacrylate resin; shaping in a mold; and polymerization, drying, pyrolyzing, and sintering. After comparison with two other commercial macroporous BCP materials, which were produced along different routes, it was found that conventional parameters such as porosity and pore size cannot describe a macroporous structure precisely enough for the application as tissue-engineering scaffold. Instead, permeability can be seen as an intrinsic and quantitative parameter to describe the macroporous structure of various scaffolds, because it is independent of sample size and fluid used in the test. Another parameter, the permeability/porosity ratio, provides an indication of the percolative efficiency per unit porous volume of a scaffold. Structural characterizations and permeability studies of other macroporous scaffold materials were also performed, and it was found that permeability could reflect a combination of five important parameters for scaffold: (1) porosity, (2) pore size and distribution, (3) interconnectivity, (4) fenestration size and distribution, and (5) orientation of pores. Finally, the implications of relating permeability with biological performances are also discussed.

INTRODUCTION

In the 1970s, calcium phosphate ceramic materials were studied for use as alternatives to autograft and allograft for bone repair and substitution.[1,2] During this early period, biphasic calcium phosphate (BCP) consisting of 80% hydroxyapatite (HA) and 20% tricalcium phosphate (β-TCP) was studied, although at that time it was recognized as "tricalcium phosphate"[3] and later identified by Daculsi *et al.* in 1988 as BCP.[4] Knowing that pure crystalline HA degrades slowly *in vivo* and that β-TCP degrades faster than expected, the concept of mixing those two has been studied extensively with particular attention paid to synchronizing the degradation rate with that of new bone formation.[5] The following aspects of BCP have been investigated: use as bone filler,[6] *in vitro* dissolution,[7] *in vivo* degradation,[8] as a carrier of bone marrow,[9] as a carrier of recombinant human bone morphogenetic protein 2 (rhBMP-2),[10] as a carrier of growth hormone,[11] and as a carrier of cells or scaffold for bone tissue engineering (TE).[12]

Regeneration of skeletal tissues has been recognized as a new means for the reconstruction of skeletal defects. The cell-based strategy of bone tissue engineering is to deliver osteoprogenitor cells with a vehicle (scaffold) to the sites for regeneration; in other words, to build an alternative or equivalent to autograft. Experiences from massive autograft transplantation, normally cortical bone,

[1]IsoTis NV, Bilthoven, The Netherlands.
[2]Biomaterials Research Group, Leiden University, Bilthoven, The Netherlands.

suggested that generating extra space in the transplanted cortical bone by osteoclasts take place before any new bone apposition.[13] The viability of the transplanted bone depends on the rapid revascularization. That understanding has resulted in the emergence and development of microsurgery. Clinical outcomes from allograft also suggested that drilling holes in the allograft may improve subsequent bony ingrowth.[14]

Similar applications for TE bone constructs determined the scaffold to be in a porous form. In this form large numbers of cells can be delivered, and vital nutrient supply becomes possible by vasculature ingrowth. From a structural viewpoint, TE bone constructs investigated more closely resemble cancellous bone than cortical bone: a porous matrix with a layer of osteoprogenitor cells. Porous ceramic scaffolds, such as hydroxyapatite,[15] BCP,[12] and coral,[16] have attracted wide interests because of their excellent biocompatibility and bioactivity in exerting positive influence on the cells/tissue carried. BCP is promising because of the advantages mentioned earlier. There are a number of methods to obtain porous BCP ceramics, generally divided into two categories: (1) from natural resources (such as coral or natural bone) by double-negative replication,[17] direct conversion,[18] or stereo lithography apparatus (SLA),[19] or (2) from complete synthetic processing. The synthetic methods can also be divided into two groups: firing powder[20] and firing slurry. Using slurry to produce porous BCP can be divided into several subcategories: (1) foaming,[21] (2) using template to obtain a negative replica,[22] and (3) using a polymeric sponge to obtain a positive replica of the reticular foam.[23] In general, all the processing routes were developed from a desire to emulate the ideal structure of natural cancellous bone. Nevertheless, the porous BCP materials obtained via these various synthetic routes are still not close enough to this ideal structure and, therefore, new attempts are continuously being tried. A novel method of preparing macroporous BCP by dual-phase mixing has been developed in our laboratory. Water-based BCP slurry was mixed with polymer resin (polymethylmethacrylate, PMMA) and the mixture was shaped in a mold, cured and dried, pyrolyzed, and sintered to a macroporous BCP ceramic.

One question was raised during the characterization of this macroporous BCP: How are different porous structures to be evaluated or compared? Conventionally, porosity (in vol%) and pore size (mean value and distribution) are used as characteristic parameters. However, further studies relating the porosity of macroporous BCP ceramics to their biological or clinical performance have led to confusion. Toth *et al.* mentioned that the ability for bone ingrowth increases when the porosity of the ceramic is increased[24] but found that after 6 months the union rates of BCP implants with 30, 50, and 70% porosity were the same. Gauthier *et al.* confirmed that no significant differences in bone ingrowth were found between implants of macroporous BCP with 40 and 50% porosity in a rabbit femoral model.[25] Rohanizadeh *et al.* revealed that fluid circulation and the interaction of ceramics with proteins or cells affect the physicochemical dissolution–reprecipitation process.[26] Does any relation exist between the porosity of a scaffold and its fluid conductance?

Either as an implant or as a scaffold for TE bone, the involvement of macroporous BCP with the circulation of body fluid or bone marrow is inevitable for new bone formation. Related work from Hui *et al.* showed that fluid conductance of cancellous bone allograft is a deciding factor in graft–host union.[27] In the current study, the permeability of the BCP produced by dual-phase mixing was studied, together with other two commercial BCP materials, to reveal the relationship between permeability and porosity. As a result, a more suitable and quantitative parameter in describing macroporous structure of TE bone scaffolds is suggested. Before we proceed, several definitions are to be clarified as listed in Table 1. The term "interconnection" is not used because of its vague meaning; instead, interconnectivity and fenestration are used.

MATERIALS AND METHODS

Scaffold processing routes

Commercial scaffolds. Two commercial scaffolds were examined: the Zimmer BCP (Z-BCP, Triostie; Zimmer, Rungis, France) and the Dytech BCP (D-BCP; Dytech, Sheffield, England). Z-BCP was produced by dry state compression of BCP powder with naphthalene particles as pore precursors.[28] The BCP powder was obtained by mixing HA and β-TCP powder. Naphthalene particles (52.5 wt%; density, 1.15 g/cm^3) were added to the BCP powder and the mixture was compacted into blocks under pressure. The blocks were then subjected to pyrolysis (550°C in N_2) and sintering (1150°C in air) processes. The use of N_2 in the pyrolysis step was because naph-

Table 1. Definitions of Parameters Involved in Describing Macroporous Structure

Parameters	*Definition*
Porosity	Percentage of volume of voids over total volume (voids + solid)
Pore	Cell space of a void
Pore size	Diameter of a spherical pore or cylindrical channel
Interconnectivity	Extent of a pore connected with its neighbors
Fenestration	Window between adjacent pores

thalene can attack the alumina tube in the furnace at temperatures of 900°C and above.[28] D-BCP was produced by a foaming slurry method.[29] The ceramic slurry was prepared by homogeneously mixing the ceramic powders, water, and a surfactant. The slurry was then transferred to a Büchner funnel with many small pores. Foaming was initiated by introducing nitrogen bubbles. After a predetermined time the foaming was stopped and the foamed construct was transferred to a filter paper box and dried further. After drying, the green body was calcined and later sintered.

Experimental scaffold: IsoTis BCP. I-BCP (IsoTis, Bilthoven, The Netherlands) was produced by a more recently developed method: dual-phase mixing. The water-based BCP slurry was mixed with PMMA resin composed of PMMA powder and MMA monomer. To obtain porosities higher than 50% for the final ceramic, small amounts of naphthalene particles were also added to the mixture. The mixture was then subjected to shaping in a mold, polymerization, drying, pyrolyzing, and sintering. The procedure is illustrated in Fig. 1.

Raw materials preparation: The raw powders of HA and β-TCP were commercially obtained from Merck (Eurolab BV, Amsterdam, The Netherlands) and BDH (Poole, England) respectively. They were calcined at 1000°C for HA and 800°C for β-TCP at a heating and cooling rate of 100°C/h without a holding stage. Polymethylmethacrylate (PMMA) powder (Dentalbiolux International, Belgium) was mixed with 1% benzoyl peroxide (BPO; Merck), which served as a radical polymerization initiator. Methylmethacrylate (MMA) monomer (Merck) was mixed with 2% *N,N*-demethyl-*p*-toluidine (DMPT; Aldrich, Milwaukee, WI), acting as accelerator for the polymerization. Particle sizes of HA powder and PMMA powders were measured in dry state, using incoherent light diffraction (Retsch Technology, Haan, Germany). Naphthalene (Aldrich) was used in the form of crystals and flakes. They were sieved and particles between 600 and 1100 μm were selected to achieve the desired final pore size in ceramic.

The BCP slurry was prepared with the following chemical composition: 28.6 wt% demineralized water and 67.3 wt% calcined HA/TCP (60/40 by weight) powder. The remainder consisted of ammonia solution (25%; Merck), defloculant (Dolapix, Aschimmer, and Schwarz, Germany) and binder (carboxy-methyl cellulose, CMC, Pomosin BV, Bunschoten, The Netherlands).

Mixing of all the ingredients: BCP slurry, naphthalene particles, MMA monomer, and PMMA powder were mixed homogeneously with a spatula in a Teflon or polyethylene (PE) beaker. The volume ratio of BCP slurry to MMA/PMMA mixture was 1:1. The addition of naphthalene (10 wt%) was necessary only if a higher porosity (>50%) was wanted. After that, the mixture was moved into PE or stainless steel molds (Φ 40 × 50 mm). After drying overnight the mold was removed. Samples were dried further at room temperature or in an oven at 50°C until they were completely dry and no further weight loss was observed.

Pyrolysis of organic phases (PMMA, naphthalene, and binder): Removal of naphthalene, PMMA, and other binders was performed in a furnace (Nabertherm 1100; Nabertherm, Lilienthol, Germany) in air under a controlled heating rate to prevent blistering, cracking, or delamination caused by (1) mismatching of thermal expansion between BCP and organic phase or (2) expansion of exhaust gases. To optimize the heating profile, thermogravimetry analyses (TGA; PerkinElmer, Norwalk, CT) were performed on pure naphthalene, PMMA, and mixture of naphthalene with BCP/PMMA. On the basis of the TGA studies, a heating profile of pyrolysis was selected as

$$\text{RT} \xrightarrow{150\ \text{min}} 150^\circ\text{C} \xrightarrow{600\ \text{min}} 350^\circ\text{C} \xrightarrow{90\ \text{min}} 440^\circ\text{C} \xrightarrow{210\ \text{min}} \text{RT}$$

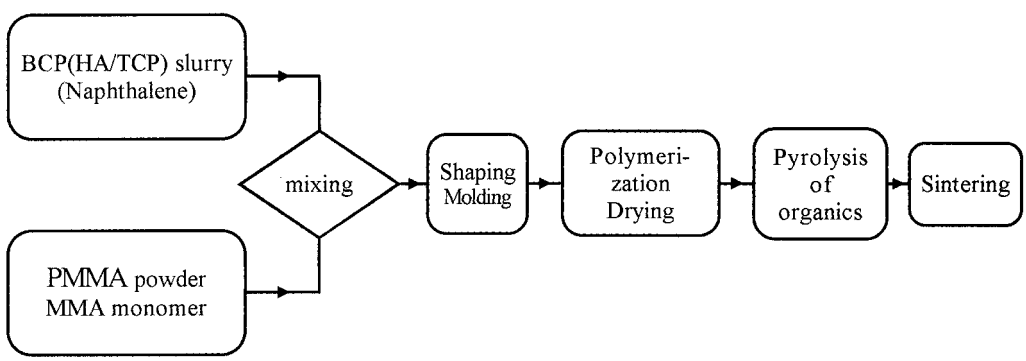

FIG. 1. Flowchart showing the processing route of BCP with dual-phase mixing method.

Sintering: After all the organic components were removed at ~440°C, the samples were finally sintered at 1250°C for 8 h in air or in N_2 atmosphere in a high-temperature furnace (HT-1600-GT-VAC, Linn High Therm, Eschenfelder, Germany).

Characterizations of scaffolds

Material characterizations were performed on I-BCP by Fourier transform-infrared spectroscopy (FT-IR) (Spectrum 1000; Perkin Elmer) and X-ray diffraction (XRD) (Miniflex; Rigaku, Tokyo, Japan).

Geometric characterizations of the porous structures of the three kinds of BCP materials were conducted. The following techniques were used: (1) 2-D image analyses (optical microscopy, scanning electron microscopy [SEM], and micro-CT [computed tomography]); (2) 3-D measurement (micro-CT and mercury intrusion porosimetry [MIP]); and (3) comprehensive 3-D evaluation (permeability study).

Macroporous structure was observed with a stereo optical microscope (Nikon SMZ-10A) equipped with a CCD camera (Sony Progressive 3CCD color video camera). For direct observation and measurement of the macroporous structures, micro-CT scanning was performed with a SkyScan-1072 high-resolution desktop microtomograph (SkyScan, Aartselaar, Belgium). Three BCP cubic samples with a size of 5 mm were measured, and a slice thickness of 10 μm. The macroporous structure and microtexture of the inner surface of pores were studied by environmental scanning electronic microscopy (ESEM) (XL 30 ESEM-FEG; Philips; Eindhoven, The Netherlands). The MIP studies were performed on the three kinds of samples by using Pascal 140 (Thermo Finnigan, Milan, Italy) and the results of mean pore size and porosity were automatically calculated with the integrated software.

The porosity and pore size of Z-BCP, D-BCP, and I-BCP were all measured. To measure the pore size, a piece of porous BCP was sawed with a diamond saw and then the cross-section was polished with a series of SiC sand papers. After cleaning in an ultrasound water bath and drying, the cross-section was colored with stamp ink (Stationery Factory 4, Tianjin, China). This stained cross-section was digitized directly by using a desktop scanner. The image obtained was used for pore size measurement by image analysis. Total porosity was determined from relative densities, by comparing the bulk density of a cylindrical sample with theoretical values: 3.156 g/cm^3 for HA and 3.07 g/cm^3 for β-TCP.

Permeability studies

The permeability studies were performed by a method described elsewhere,[30] in which a fluid under a known pressure is allowed to flow through the porous specimen and the flow rate is measured. Measurement was repeated five times for each kind of material. Samples were prepared in the shape of either a rectangular bar or a cylinder, with a length of 20 mm. A piece of rubber tube was used to connect the sample with a fluid reservoir (inner diameter, 13.38 cm). All specimens were mounted in a polystyrene (PS) tube (20 mm in length). The space between samples and the PS tube was sealed with Parafilm. The pressure at the bottom surface of the specimen was zero, while the pressure at the top surface was generated by the water level between the reservoir and specimen top surface. In this study it was 143.4 cm, corresponding to a pressure of 14.07 kPa. Demineralized water was selected as the fluid. A maximum flow volume of 80 mL was used, resulting in a 5.7-mm drop in fluid level and a negligible pressure drop of 0.4% of the original pressure. The volumetric flow rate (mL/s) through the specimen was measured by determining the volume of water

Table 2. Porous Ceramic Scaffolds Tested for Their Permeabilities

Material	*Description*
Z-BCP	Porous BCP form Zimmer. Porosity = 75%
D-BCP	Porous BCP form Dytech. Porosity = 80%
I-BCP	Porous BCP produced at IsoTis. Porosity = 60%
HA-60	Porous HA produced by dual-phase mixing method. Porosity = 60%
HA-60(O)	Porous HA produced by dual-phase mixing method with pores being orientated. Porosity = 60%
HA-60(S)	Similar to HA-60 with smaller pores. Porosity = 60%
HA-50	Porous HA produced by dual-phase mixing method. Porosity = 50%
Coral	*Goniopore*, harvested from South China Sea. Porosity = 60%
ProOsteon 500	Commercial product from Interpore-Cross. Porostiy = 68%
HA-CAM	Porous HA commercially obtained from CAM BV (Leiden, The Netherlands). L, Along laminar porous direction; P, perpendicular to laminar direction. Porosity = 70%
Bone (H,T)	Human proximal femur in transverse direction, with 73% porosity[a]

[a]See Ref. 30.

that had flowed through the specimen into a 100-mL graduated cylinder in a span of time measured with a Seiko stop watch (accuracy of 0.1 s). The conductance (C) of fluid flow through the specimen was calculated as

$$C = \Delta Q/\Delta P \quad (1)$$

where ΔQ is the induced flow (mL/s) and ΔP is the pressure drop (kPa) across the specimen. Applying Darcy's law[31] to the specimen, we obtained the conductance as

$$C = A\kappa/L\mu \quad (2)$$

where A and L are the cross-sectional area (cm^2) and length (cm) of the sample, respectively, κ is permeability, and μ is kinematic fluid viscosity (η/ρ), where the viscosity (η) of water is 0.001 Pa • s.[32]

Combining Eqs. (1) and (2), the permeability can be calculated as

$$\kappa = \Delta QL\mu/(\Delta PA) \quad (3)$$

To verify whether permeability can be used as an indicative parameter of the macroporous structure, reflecting porosity, pore size, pore distribution, interconnectivity, fenestration size, fenestration distribution, and orientation of

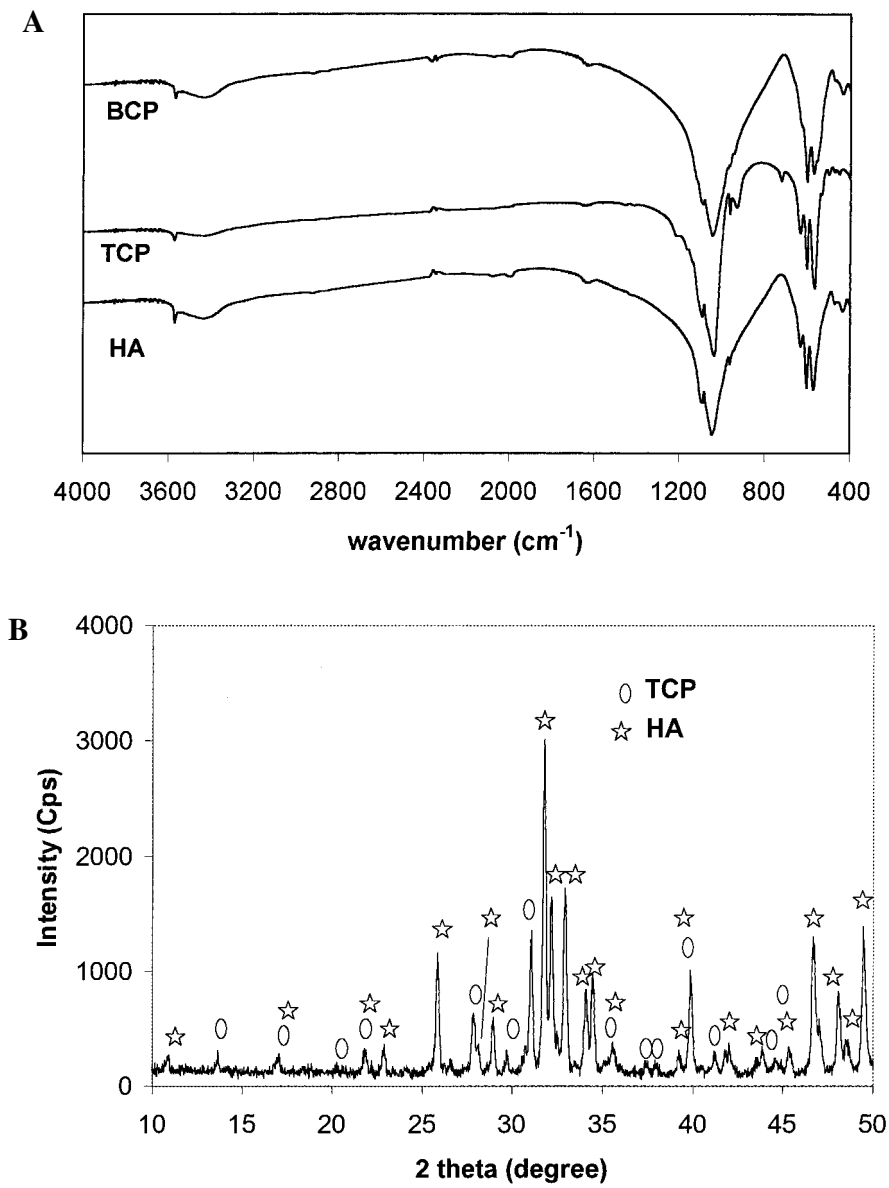

FIG. 2. (**A**) FT-IR spectra of HA, β-TCP, and I-BCP; (B) XRD spectrum of I-BCP.

pores, various ceramic scaffolds with different porous structures were studied as listed in Table 2.

RESULTS

Processing of I-BCP

Particle size of HA, β-TCP, and PMMA. By calcination, the mean particle size of both HA and β-TCP powder increased slightly. Another effect of calcination was the decrease in specific surface area (SSA) of HA powder, as the result of particles fusing together. The majority of the PMMA particles (~50%) ranged between 10 and 30 μm in size. The detailed distribution chart is not shown here.

Pyrolysis of organic phases. The TGA results showed that naphthalene tends to sublimate: holding at 50°C, a small amount of naphthalene will change into gas. With further heating, it disappeared as gas completely below 150°C. The TGA curve of the BCP/PMMA/naphthalene mixture showed that most of the PMMA resin pyrolyzed between 250 and 350°C. To complete this pyrolysis process, it was heated to 440°C. During the whole pyrolysis process, no combustion of PMMA in air was observed.

Shrinkage of porous HA. Assuming the diameter of a sample after demolding was D, then after pyrolysis the diameter was $0.994D$ and after sintering it was $0.768D$. Therefore, the linear shrinkage rate is 23%, corresponding to a volumetric decrease of about 50%.

Material characterization of I-BCP

The FT-IR spectra of HA, β-TCP, and I-BCP after sintering are shown in Fig. 2A. It is clearly shown that I-BCP is composed of HA and β-TCP and no other phases, that is, CaO or α-TCP, were found. The composition of BCP is confirmed by its XRD spectrum as in Fig. 2B. BCP produced in this study is highly crystalline. According to the producer, Z-BCP is composed of HA and TCP with a weight ratio of 60/40, whereas D-BCP has 60 ± 5% of HA in HA/TCP.

Macroporous structural characterization of three BCP materials

The results of the characterizations of the three porous structures are summarized in Table 3. The images of their macroporous structures (optical, SEM, and micro-CT) are shown in Fig. 3, indicating clearly different features. Z-BCP has many irregularly shaped pores that were generated by naphthalene particles. The isostatic compaction of naphthalene particles with BCP powder did not establish many interconnective channels between naphthalene particles, resulting in isolated pores. From 2-D image observation and micro-CT scanning, the fenestrations are either too small (e.g., less than 100 μm) or nonexistent. The sizes of pores and total porosity were well controlled. In this case, the pore size is 565 ± 33 μm and the porosity is 75%.

D-BCP possesses a different macroporous structure. Pores are generally open, interconnected, and distributed in a wider range compared with Z-BCP. Because of the foaming process some pores grew to more than 1000 (m, as shown at the bottom of the ESEM image in Fig. 3. In most cases, pore are well interconnected through fenestrations with (much) smaller sizes than pores. Average pore size was measured as 300 μm and pores ranged from 50 to 500 μm.

The macroporous structure of I-BCP was different from those of Z-BCP and D-BCP. The traditional concept of a *pore* as a void was not appropriate in describing the morphology of this porous structure; instead, "intermingled channels" better describes the real situation. In this case, the width or diameter of the channel was taken as the pore size. The results of such measurements from 2-D images indicated that the average pore size is 441 μm with more than 90% of pores ranging from 200 to 900 μm.

Table 3. Structural Characteristic Results of Three BCP Materials

	Z-BCP	*D-BCP*	*I-BCP*
Processing routes	Solid compression with fugitive naphthalene particles	Foaming: introducing nitrogen bubbles into BCP slurry	Dual-phase mixing: HA/TCP slurry with PMMA/MMA resin
Pore size (μM) from 2-D image analysis	Mean, 565; range, 532–598	Mean, 300; range, 50–500	Mean, 528; range, >90%, 200–900
Mean pore size (μm) from MIP	29	262	523
Porosity (%) from density calculation	74.5	78.3	60.2
Porosity (%) from MIP	0.76	70	48

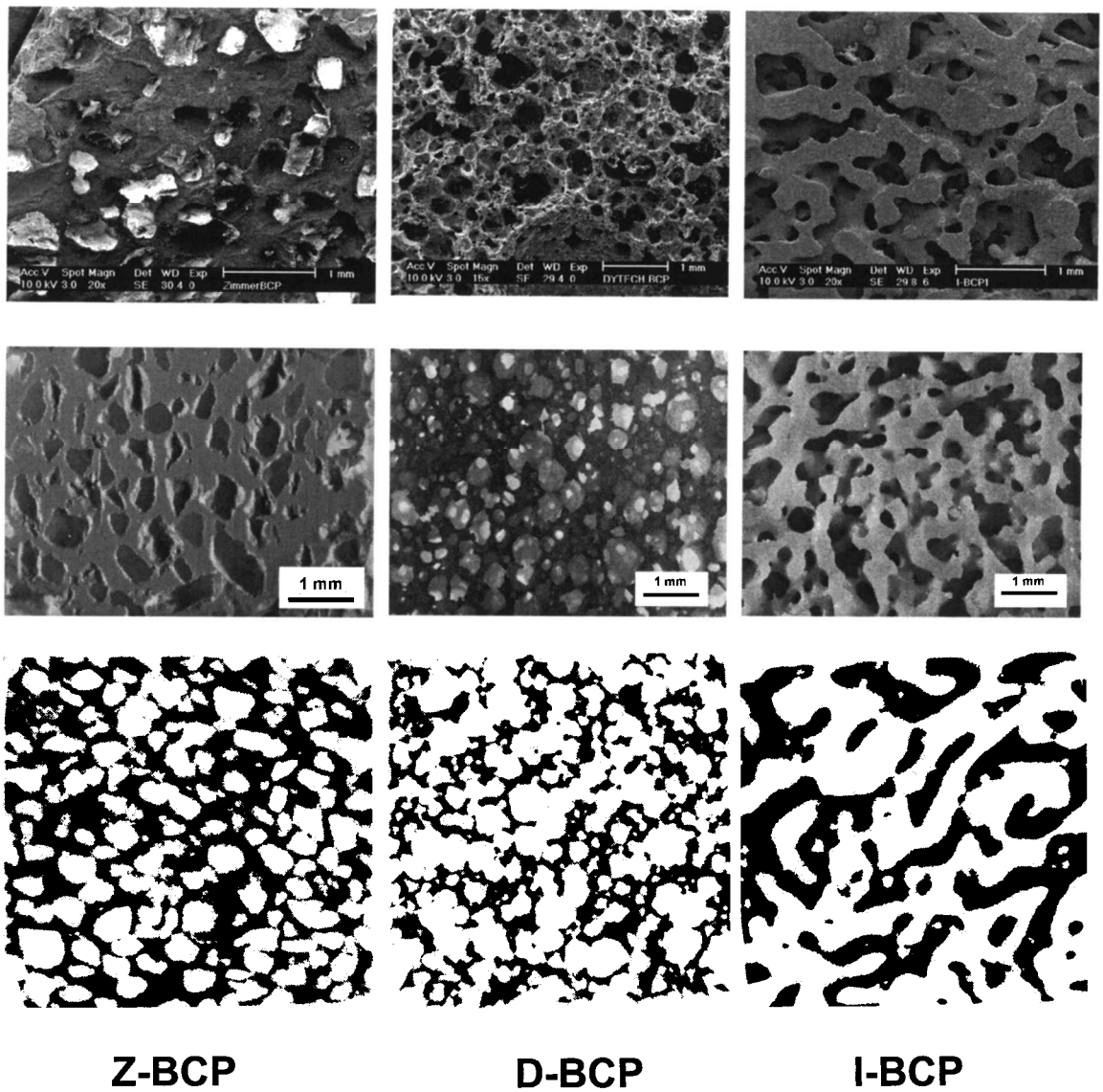

FIG. 3. Images showing the macroporous structures of Z-BCP, D-BCP, and I-BCP. *Top*: ESEM pictures. *Middle*: Optical pictures. *Bottom*: Cross-sectional images extracted from micro-CT scanning (size of the square section is 5 mm).

MIP measurement. The results of mercury intrusion of the three materials are shown in Fig. 4. The distribution of pore size showed different modes for different materials. Z-BCP has a bimodal pore size distribution with peaks around 30 μm (10–90 μm) and 200–800 μm. D-BCP has a more regular distribution, the majority being located around 300 μm. I-BCP is similar to D-BCP, but with larger pore size; the majority are located in the range of 400 to 800 μm. The fact that the MIP measurements showed different results in both mean pore size (compared with those from 2-D image analyses) and porosity (compared with those from density calculation and micro-CT) requires explanation. Because of the inaccessibility of the inner pores in Z-BCP, both mean pore size and porosity determined by MIP are not reliable. Also, because the MIP method cannot measure pores greater than 800 μm, the porosity of both D-BCP and I-BCP determined by MIP showed lower values compared with the calculated data.

Microporous structural characterization of the three BCP materials

The microstructures of the inner surfaces of pores are shown in Fig. 5. In comparing D-BCP with I-BCP under low magnification, I-BCP showed a slightly rougher surface throughout. Under higher magnification no differences were observed. For both D-BCP and I-BCP, all

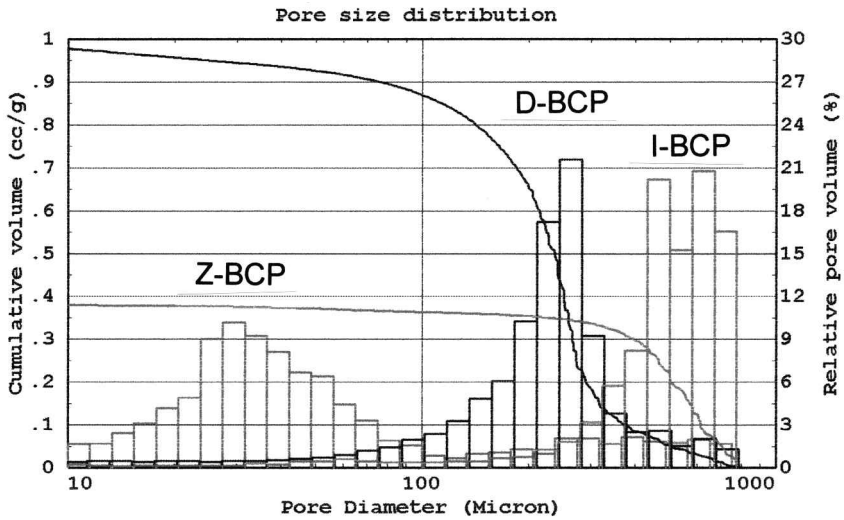

FIG. 4. Results of mercury intrusion of three BCP materials, showing the distribution of pore sizes (more accurately, fenestration sizes).

grains were highly fused and most grains were much larger than 1 μm. Z-BCP had a clearly different microsurface pattern. Under higher magnification it was observed that the raw powders were sintered together, but there were still spaces on the order of 1 μm left between those particles.

Permeability and permeability/porosity ratio of three BCP materials

After calculation, the permeability data and permeability/porosity ratio for the three BCP samples are illustrated in Fig. 6. Of the three materials, I-BCP has the highest permeability, 3.5 times that of D-BCP and 19 times that of Z-BCP. Taking porosity into consideration, I-BCP possesses the highest permeability/porosity ratio, indicating that I-BCP achieved the highest percolative efficiency per unit porous volume.

Relations between macroporous structure and permeability

The permeabilities of other scaffold materials with different macroporous structures are given in Fig. 7. For comparison of their structures, optical microscopy images are shown in Fig. 8. Some characteristic information and porosity data are given in Table 2 and pore size distributions are shown in Fig. 9. The results indicated that, in actuality, permeability is affected by a combination of (1) porosity, (2) pore size and distribution, (3) interconnectivity, (4) fenestration size and distribution, and (5) orientation of pores with respect to flow direction.

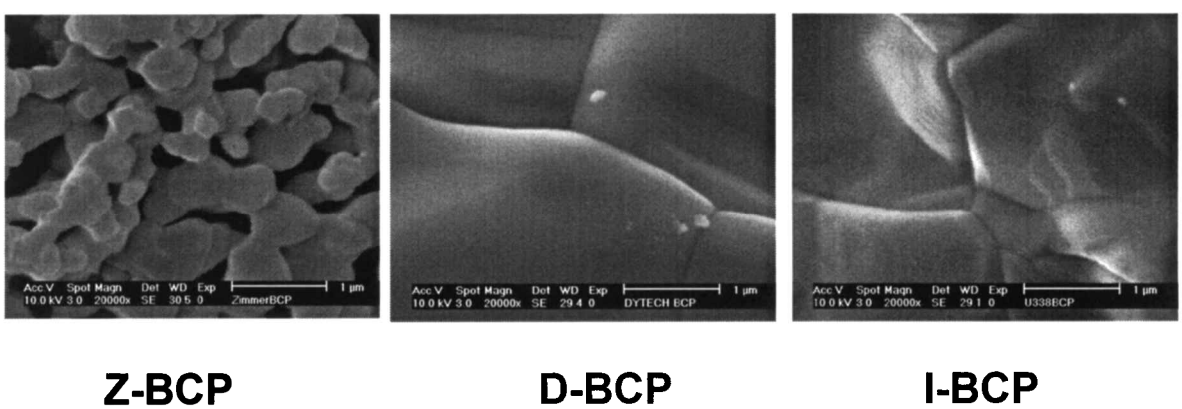

FIG. 5. Microstructural images of the three BCP materials studied.

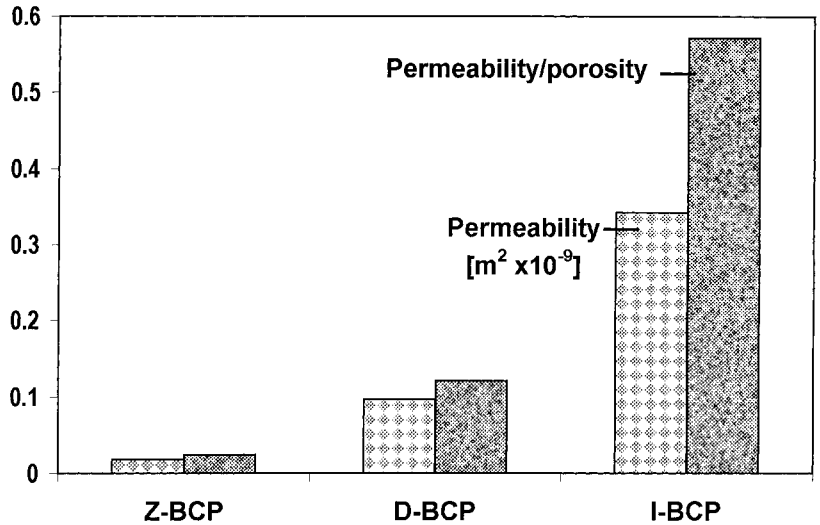

FIG. 6. Permeability and permeability/porosity ratio of the three BCP materials studied.

DISCUSSION

Porosity, pore size (mean value and range) are inappropriate parameters in describing the accessibility of inner voids

The purpose of the current study was not to rank different BCP materials, because the evaluation of biomaterials depends not only on their macroporous structures but also on their biological and clinical performances. Instead, this study was triggered by the fact that when, in attempts to compare or evaluate different scaffolds for TE bone from different experiments in the same group or between different groups, inconsistent results were usually found. Besides the many parameters encountered in biological procedures, such as media contents, cell culture parameters, seeding methods, seeding density and seeding efficiency, and so on, the scaffold itself has many parameters as well. Important, even critical, parameters such as pore size distribution, porosity, interconnectivity, fenestrations and specific surface area are not always presented in publications. The difficulty of assessing some of these parameters might be the reason for this lack of data. Therefore, it would be interesting to have a more accessible way of qualifying the properties of porous

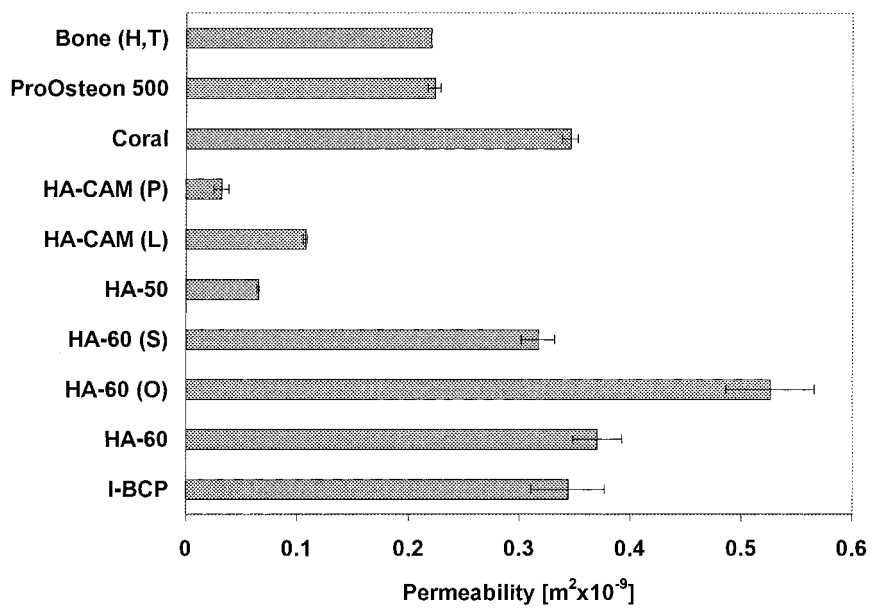

FIG. 7. Permeability results for various scaffolds, indicating the change in several structural parameters such as porosity, pore size, fenestration, orientation, and interconnectivity.

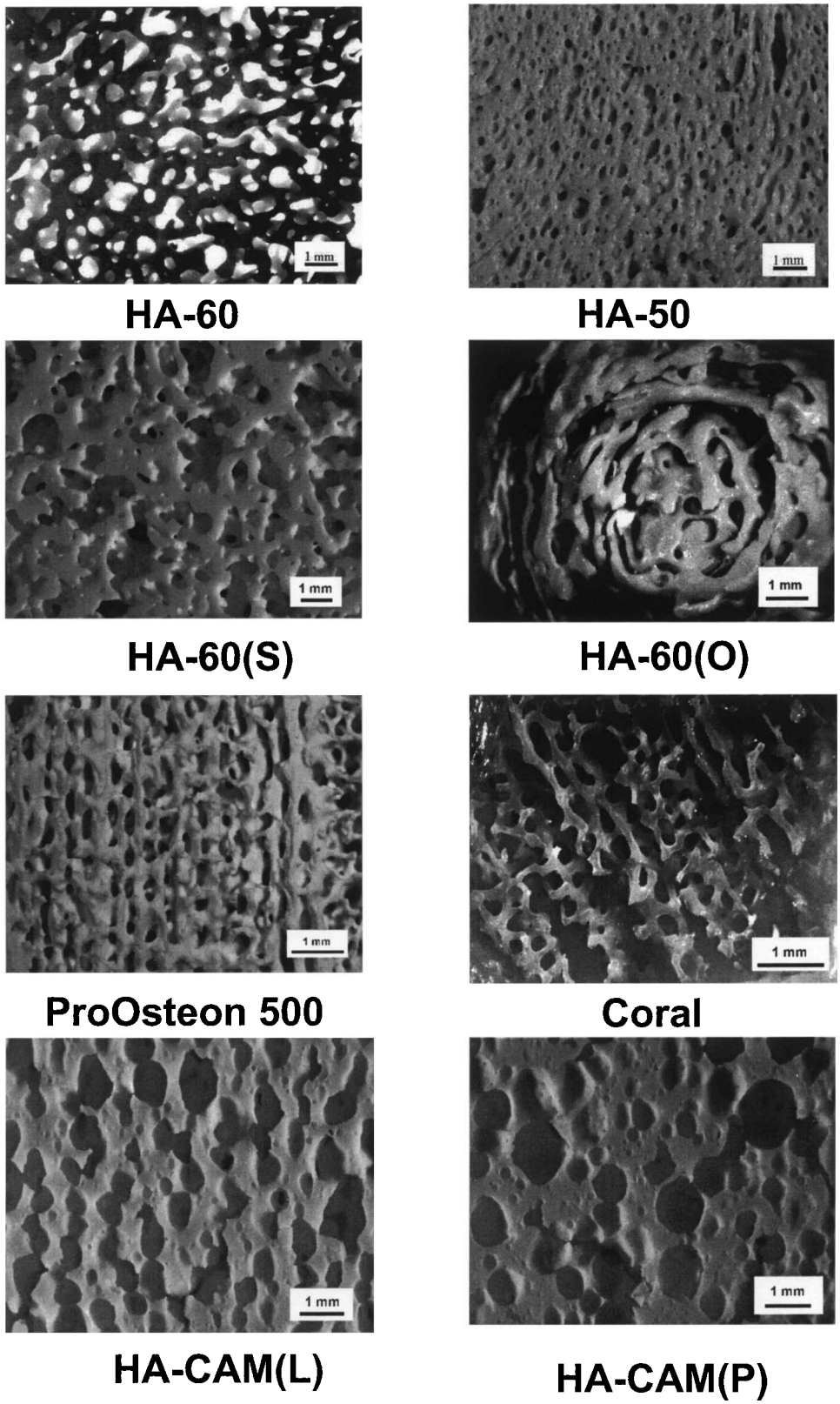

FIG. 8. Macroporous structures of various scaffolds.

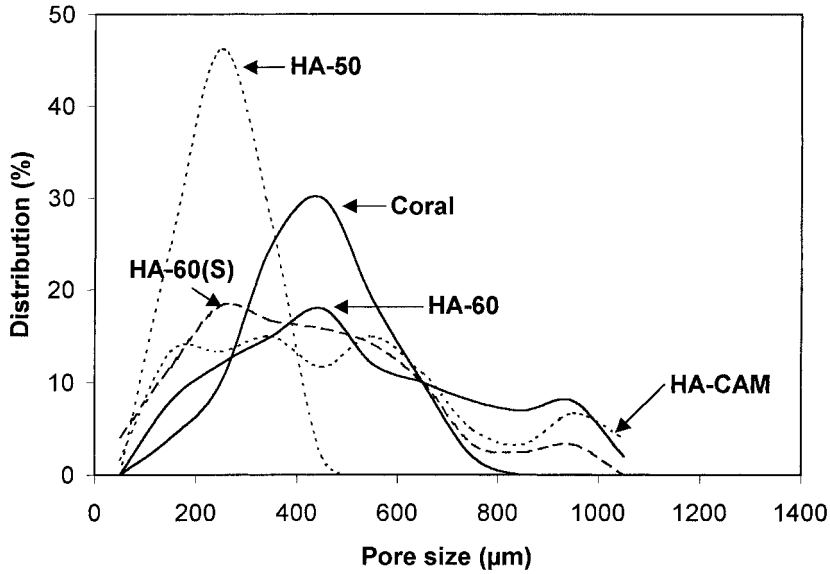

FIG. 9. Pore size distribution of various scaffolds.

structures beyond the usual porosity and pore size alone while avoiding the need to use mercury porosimetry.

It is not feasible to ask each biologist or surgeon to provide so many parameters of their scaffolds used. Therefore, it would be interesting and useful to know how different scaffolds can be evaluated. The results of the current study demonstrated that a porous scaffold with porosity higher than 70% could have low permeability or, in other words, poor accessibility, if the pores are not well connected (like Z-BCP) or connected through small fenestrations (like D-BCP). We found that BCP scaffolds can be evaluated quantitatively in terms of permeability. However, a scaffold with high permeability and low porosity is not necessarily optimal for bone TE application. On the other hand, mechanical strength is not favored by high porosities. Keep in mind that the compressive strength will be decreased with increasing porosity[33]; therefore, it seems that the permeability/porosity ratio is the better parameter to characterize porous scaffolds for tissue-engineering purposes.

The three kinds of BCP in this study have similar mean pore size and porosity. Why did I-BCP have the highest permeability, when it possesses the lowest porosity? It is the result of its macroporous structure, generated by the novel processing technique of dual-phase mixing. The two starting phases, namely water-based BCP slurry (naphthalene containing) and organic PMMA resin, penetrate and intermingle during mixing while retaining the continuity of each phase. Therefore all the pores (the former acrylic phase), in principle, are open. The interconnectivity depends heavily on the proportion of PMMA in the mixture as it determines the probability of one part of PMMA to meet and coalesce with another part. The nature of this procedure explains the formation of channel-shaped pores and less discrepancy between fenestration size and pore size. Higher permeability can thus be achieved.

Compared with the other processing routes, dual-phase mixing also has the advantage of good workability. Experiments showed that the shape of the pores in porous HA made by the dual-phase mixing method can be adjusted and oriented.[34] Scaffolds produced in such a way have potential application in sites where different permeability in different directions is preferred.

Permeability is a representative and comprehensive parameter in describing macroporous scaffolds quantitatively

The influence of porosity on permeability can be revealed by comparing HA-60(S) and HA-50. The comparison of HA-60 with HA-50 showed that a 10% increase in the porosity resulted in a significant increase in permeability: for both HA-60 and HA-60(S), their permeabilities were at least twice that of HA-50. Thus, a positive correlation exists between porosity and permeability, provided that most pores are well interconnected, as in natural bone.[30,32] In comparing HA-60 with HA-60(S), we can conclude that for the same porosity, a structure with smaller pore size possesses a lower permeability clearly as a result of higher total pore surface, and thus higher friction force between fluid and material.

HA-60(O) and HA-60(S) were produced in the same batch, but the former was subjected to shear stress before hardening and therefore its pores were oriented and

elongated. As a result, higher permeability was measured along the elongated direction.

It is necessary to point out that the "permeability" mentioned above actually means Darcian permeability. This is based on two facts: (1) non-Darcian permeability is less dependent on the macroporous structure compared with Darcian permeability; and (2) at low flow rate (Re $>>$ 1, where Re is the Reynolds number), it is accurate enough to use Darcy's law to measure permeability.[35]

Implication of relating permeability of a scaffold with biological performances

Another question may be raised: If permeability is a more "comprehensive" parameter in describing macroporous structure, as shown in this study, is there any relationship between permeability and biological and clinical performance? The relationships between the permeability of a scaffold and its biological or clinical performance can be exploited *in vitro* and *in vivo*. *In vivo* studies include using porous scaffold alone (similar to autograft, allograft, and synthetic implants), or using porous scaffold to carry cells/tissue.

In vitro *studies.* Compared with implants, one extra requirement for TE scaffolds is that they need to cope with cell seeding *in vitro.* In essence, this is a perfusion process with cell-containing fluid. It is well known that permeability is measured in a perfusion process.[36]

In vivo *studies: scaffold alone.* As mentioned earlier, for cortical autograft, increasing permeability favors new bone formation. The fluid conductance of a specimen is defined as the ratio of induced fluid flow (fluid volume per unit time, mL/s) to its pressure drop (kPa) across the specimen. Hui *et al.* reported a threshold conductance to achieve union for freeze–dried cancellous bone allografts from porcine femoral heads implanted into tibia segmental defects of 29 rabbits.[27] Below this threshold, sufficient revascularization could not be attained. This is because bone repair and healing is a size-dependent process,[37] as is fluid conductance. This may explain why a direct relation is found between the two. Permeability could be considered as the conductance normalized by the geometric size of the sample tested and the viscosity of fluid used. In other words, permeability is a specific property of macroporous materials, independent of sample size and the fluid used in the tests. Therefore, it is more suitable to use permeability than fluid conductance for characterization of a macroporous implant or scaffold.

For synthetic implants, several investigators have shown that there exists a pore size threshold for tissue ingrowth: no tissue grows in pores smaller than 5 μm, fibrous tissues will grow in 5- to 15-μm pores, osteoid tissue can occur in pores of 40–100 μm, and mineralized bone needs pores larger than 100 μm.[38] The governing role of fenestration in permeability was proved in the current study. The threshold of permeability for the ingrowth of various tissues needs to be studied further.

CONCLUSIONS

A novel processing method of dual-phase mixing was used to produce macroporous biphasic calcium phosphate. The obtained BCP has a porosity of 60% and a fully interconnected porous structure. Its channel-shaped pores are different from those of other synthetic BCP materials. Also, this obtained BCP has the highest permeability and permeability/porosity ratio compared with two commercial BCP scaffolds.

The permeability was a result of the combination of (1) porosity, (2) pore size and distribution, (3) interconnectivity, (4) fenestration size and distribution, and (5) orientation of pores with respect to flow direction. Permeability can be taken as a comprehensive intrinsic parameter in describing macroporous structures. This is especially important for TE scaffolds, for which fluid flow is critical *in vitro* and, later, *in vivo*. It is suggested that permeability is more relevant than porosity and mean pore size in characterizing the scaffold for (bone) tissue engineering. From a practical point of view, permeability can be easily measured without any specific instrumental requirements.

ACKNOWLEDGMENTS

The authors thank Fabienn Peters for enthusiastic help in the TGA experiments; Dr. ir. Harrie Weinans (Erasmus University, Rotterdam) for help in the micro-CT tests; Prof. Yang, WeiDong (Fourth Military Medical University, China) for providing the coral samples; and Mr. P. Riva for performing the MIP measurement.

REFERENCES

1. Levin, M.P., Getter, L., and Cutright, D.E. A comparison of iliac marrow and biodegradable ceramic in periodontal defects. J. Biomed. Mater. Res. **9,** 183, 1975.
2. Rejda, B.V., Peelen, J.G., Vermeiden, J.H., and De Groot, K. Tri-calcium phosphate as a bone substitute. J. Bioeng. **1,** 93, 1977.
3. Nery, E.B., Lynch, K.L., Hirthe, W.M., and Mueller, K.H. Bioceramics implants in surgically produced infrabony defects. J. Periodontol. **46,** 328, 1975.
4. Daculsi, G., Le Geros, R.Z., and Deudon, C. Scanning and transmission electron microscopy, and electron probe analysis of the interface between implants and host bone: Os-

seo-coalescence versus osseo-integration. Scanning Microsc. **4,** 309, 1990.
5. Ellinger, R.F., Nery, E.B., and Lynch, K.L. Histological assessment of periodontal osseous defects following implantation of hydroxyapatite and biphasic calcium phosphate ceramics: A case report. Int. J. Periodontics Restorative Dent. **6,** 22, 1986.
6. Moore, D.C., Chapman, M.W., and Manske, D. The evaluation of a biphasic calcium phosphate ceramic for use in grafting long-bone diaphyseal defects. J. Orthop. Res. **5,** 356, 1987.
7. Ducheyne, P., Radin, S., and King, L. The effect of calcium phosphate ceramic composition and structure on in vitro behavior. I. Dissolution. J. Biomed. Mater. Res. **27,** 25, 1993.
8. Hashimoto-Uoshima, M., Ishikawa, I., Kinoshita, A., Weng, H.T., and Oda, S. Clinical and histologic observation of replacement of biphasic calcium phosphate by bone tissue in monkeys. Int. J. Periodontics Restorative Dent. **15,** 205, 1995.
9. Grundel, R.E., Chapman, M.W., Yee, T., and Moore, D.C. Autogeneic bone marrow and porous biphasic calcium phosphate ceramic for segmental bone defects in the canine ulna. Clin. Orthop. **266,** 244, 1991.
10. Oda, S., Kinoshita, A., Higuchi, T., Shizuya, T., and Ishikawa, I. Ectopic bone formation by biphasic calcium phosphate (BCP) combined with recombinant human bone morphogenetic protein-2 (rhBMP-2). J. Med. Dent. Sci. **44,** 53, 1997.
11. Guicheux, J., Kimakhe, S., Heymann, D., Pilet, P., and Daculsi, G. Growth hormone stimulates the degradation of calcium phosphate biomaterial by human monocytes macrophages in vitro. J. Biomed. Mater. Res. **40,** 79, 1998.
12. Kadiyala, S., Jaiswal, N., and Bruder, S.P. Culture-expanded, bone marrow-derived mesenchymal stem cells can regenerate a critical-sized segmental bone defect. Tissue Eng. **3,** 173, 1997.
13. Springfield, D.S. Massive autogenous bone grafts. Orthop. Clin. North Am. **18,** 249, 1987.
14. Gendler, E. Perforated demineralized bone matrix: A new form of osteoinductive biomaterials. J. Biomed. Mater. Res. **20,** 687, 1986.
15. Kon, E., Muraglia, A., Corsi, A., Bianco, P., Marcacci, M., Martin, I., Boyde, A., Ruspantini, I., Chistolini, P., Rocca, M., Giardino, R., Cancedda, R., and Quarto, R. Autologous bone marrow stromal cells loaded onto porous hydroxyapatite ceramic accelerate bone repair in critical-size defects of sheep long bones. J. Biomed. Mater. Res. **49,** 328, 2000.
16. Petite, H., Viateau, V., Bensaid, W., Meunier, A., de Pollak, C., Bourguignon, M., Oudina, K., Sedel, L., and Guillemin, G. Tissue-engineered bone regeneration. Nat. Biotechnol. **18,** 959, 2000.
17. Weber, J.N., White, R.A., and Lebiedzik, J. New porous biomaterials by replication of echinoderm skeletal microstructure. Nature **233,** 337, 1971.
18. Lin, F.H., Liao, C.J., Chen, K.S., Sun, J.S., and Lin, C.Y. Preparation of βTCP/HAP biphasic ceramics with natural bone structure by heating bovine cancellous bone with the addition of $(NH_4)_2HPO_4$. J. Biomed. Mater. Res. **51,** 157, 2000.
19. Hollister, S.J., Levy, R.A., Chu, T.M., Halloran, J.W., and Feinberg, S.E. An image-based approach for designing and manufacturing craniofacial scaffolds. Int. J. Oral Maxillofac. Surg. **29,** 67, 2000.
20. Hubbard, W.G. Physiological calcium phosphates as orthopedic biomaterials. [Ph.D. thesis]. Marquette University, Milwaukee, WI, 1974, p.169.
21. Wang, J., Chen, W., Li, Y., Fan, S., Weng, J., and Zhang, X. Biological evaluation of biphasic calcium phosphate ceramic vertebral laminae. Biomaterials **19,** 1387, 1998.
22. Richart, O., Descamps, M., and Liebetrau, A. Macroporous calcium phosphate ceramics: Optimization of the porous structure and its effect on the bone ingrowth in a sheep model. Key Eng. Mater. **192–195,** 425, 2001.
23. Woyansky, J.S., Scott, C.E., and Minnear, W.P. Processing of porous ceramics. Am. Ceram. Soc. Bull. **71,** 1674, 1992.
24. Toth, J.M., An, H.S., Lim, T.H., Ran, Y., Weiss, N.G., Lundberg, W.R., Xu, R.M., and Lynch, K.L. Evaluation of porous biphasic calcium phosphate ceramics for anterior cervical interbody fusion in a caprine model. Spine **20,** 2203, 1995.
25. Gauthier, O., Bouler, J.M., Aguado, E., Pilet, P., and Daculsi, G. Macroporous biphasic calcium phosphate ceramics: Influence of macropore diameter and macroporosity percentage on bone ingrowth. Biomaterials **19,** 133, 1998.
26. Rohanizadeh, R., Trecant-Viana, M., and Daculsi, G. Ultrastructural study of apatite precipitation in implanted calcium phosphate ceramic: Influence of the implantation site. Calcif. Tissue Int. **64,** 430, 1999.
27. Hui, P.W., Leung, P.C., and Sher, A. Fluid conductance of cancellous bone graft as a predictor for graft-host interface healing. J. Biomech. **29,** 123, 1996.
28. Bouler, J.M., Trecant, M., Delecrin, J., Royer, J., Passuti, N., and Daculsi, G. Macroporous biphasic calcium phosphate ceramics: Influence of five synthesis parameters on compressive strength. J. Biomed. Mater. Res. **32,** 603, 1996.
29. European patent, EP0598783, Dytech Corporation, Ltd.
30. Grimm, M.J., and Williams, J.L. Measurements of permeability in human calcaneal trabecular bone. J. Biomech, **30,** 743, 1997.
31. Darcy, H. Les Fontaines Publiques de la Ville de Dijon. Paris: Victor Dalmont, 1856.
32. Nauman, E.A., Fong, K.E., and Keaveny, T.M. Dependence of intertrabecular permeability on flow direction and anatomic site. Ann. Biomed. Eng. **27,** 517, 1999.
33. Gibson, L.J., and Ashby, M.F. Cellular Solids: Structure and Properties. Oxford: Pergamon Press, 1988.
34. Li, S.H., de Groot, K., and Layrolle, P. Bioceramic scaffold with controlled porous structure for bone tissue engineering. Key Eng. Mat. **218–220,** 25, 2002.
35. Innocentini, M.D.M., Sepulveda, P., Salvini, V.R., and Pandolfelli, V.C. Permeability and structure of cellular ceramics: A comparison between two preparation techniques. J. Am. Ceram. Soc. **81,** 3349, 1998.
36. Kohles, S.S., Roberts, J.B., Upton, M.L., Wilson, C.G., Bonassar, L.J., and Schlichting, A.L. Direct perfusion measurements of cancellous bone anisotropic permeability. J. Biomech. **34,** 1197, 2001.

37. Schenk, R.K., and Hunziker, E.B. Histologic and ultrastructural features of fracture healing. In: Brighton, C.T., Friedlaender, G., and Lane, J.M., eds. Bone Formation and Repair. Rosemont, IL: American Academy of Orthopedic Surgeons, 1994, pp. 117–146.
38. Hulbert, S.F., Young, F.A., Mathews, R.S., Klawitter, J.J., Talbert, C.D., and Stelling, F.H. Potential of ceramic materials as permanently implantable skeletal prostheses. J. Biomed. Mater. Res. **4,** 433, 1970.

Address reprint requests to:
Shihong Li, Ph.D.
IsoTis NV
Prof. Bronkhorstlaan 10-D
3723 MB Bilthoven, The Netherlands

E-mail: Shihong.li@isotis.com